J. metamorphic Geol., 2007, **25,** 83–96 doi:10.1111/j.1525-1314.2007.00694.x

Experimental studies of mineralogical assemblages of metasedimentary rocks at Earth's mantle transition zone conditions

L. F. DOBRZHINETSKAYA[1] AND H. W. GREEN[1,2]
[1]*Department of Earth Sciences, University of California, Riverside, CA 92521, USA (larissa@ucr.edu)*
[2]*Institute of Geophysics and Planetary Physics, University of California, Riverside, CA 92521, USA*

ABSTRACT Metasedimentary rocks, a major component of the continental crust, are abundant within ultra-high pressure (UHP) metamorphic terranes related to continental collisions. The presence of diamond, coesite, and relics of decompressed minerals in these rocks suggests that they were subducted to a depth of more than 150–250 km. Reconnaissance experiments at 9–12 GPa and 1000–1300 °C on compositions corresponding to felsic rocks from diamond-bearing UHP terranes of Germany and Kazakhstan show that at higher pressures they consist of majoritic garnet, Al-Na-rich clinopyroxene, stishovite, solid solution of $KAlSi_3O_8$-$NaAlSi_3O_8$ hollandite, topaz-OH, and TiO_2 with α-PbO_2 structure. Comparison of our data with experiments conducted by others at similar *P–T* conditions shows differences, which are due to variations in bulk chemistry and the type of starting material (gel, oxides, minerals). These differences may affect correct establishment of the 'point of no return' of subducted continental lithologies. This paper discusses the implication of the experimental data with regard to naturally existing UHP metamorphic rocks and their significance for our understanding of the deep subduction of continental material.

Key words: multianvil experiments, granite, high pressure.

INTRODUCTION

Geology textbooks indicate that continental crust cannot be subducted deeply into the Earth's mantle. The arguments are as follows: 'whereas oceanic lithosphere is relatively dense and sinks into the asthenosphere, continental lithosphere is buoyant, which prevents it from being subducted to any great depth' (Tarbuck & Lutgens, 2002), or that 'one continent may slide a short distance under another, but will not go down a subduction zone' (Plummer *et al.*, 1999). These statements are based on assumptions of the relatively low density of continental crust (2.7 g cm^{-3}) in contrast to the dense rocks of the upper mantle (3.38–3.42 g cm^{-3}) (e.g. Ringwood, 1991). Such a difference makes crustal rocks buoyant and it was thought to prevent them from being deeply subducted.

This paradigm was broken with the discovery of metamorphic rocks of continental affinities containing coesite (Chopin, 1984; Smith, 1984), diamond (Sobolev & Shatsky, 1990; Xu *et al.*, 1992; Dobrzhinetskaya *et al.*, 1995; Massonne, 1999; Mposkos & Kostopoulos, 2001; van Roermund *et al.*, 2002; Perraki *et al.*, 2006), olivine with oriented exsolutions of ilmenite and chromite, or magnetite (Dobrzhinetskaya *et al.*, 1996; Green *et al.*, 1997; Bozhilov *et al.*, 1999, 2003a; Zhang *et al.*, 1999), relics of former majoritic garnet (van Roermund & Drury, 1998; Ye *et al.*, 2000; Spengler *et al.*, 2006), and also titanite and omphacite containing exsolved coesite rods and plates (e.g. Ogasawara *et al.*, 2002; Song *et al.*, 2005). All of these mineralogical assemblages suggest that the rocks were subjected to recrystallization at high pressures and high temperatures requiring a depth of > 100–250 km. The occurrences of ultra-high pressure metamorphic (UHPM) rocks within continental collision zones corroborate the fact that light material of the continental crust, despite its buoyancy, has been subducted at least to the upper mantle, perhaps even to the mantle transition zone, and that some of it has been exhumed to the surface from those depths.

The possibility of large-scale deep subduction of continental crust was strengthened with a find of microdiamonds within Qinling gneisses and eclogites in the Central Orogenic belt of China (Yang *et al.*, 2003). This finding bridges the earlier recognized Qaidam and Dabie-Sulu UHPM terranes, thereby confirming the existence of a larger UHPM belt extending more than 4000 km in length. Although at relatively shallow depth the subduction of continental slab is limited by its buoyancy, small dismembered fragments of metamorphic and magmatic rocks composed of active continental margins and/or pelagic and terrigenous shelf sediments may be transported deep into the subduction zone by the heavier oceanic plate. Therefore, it is conceivable that in the past the process of

deep subduction of materials of continental crust and their 'recycling' into the Earth's mantle might have operated on a globally significant scale.

The idea that materials of continental crust, along with terrigenous and pelagic sediments may descend into the Earth's upper and lower mantle and create their specific geochemical reservoirs is widely supported by data on the ratio of stable isotope pairs, such as $^{2}H/^{1}H$, $^{18}O/^{16}O$, $^{87}Sr/^{86}Sr$, $^{176}Hf/^{177}Hf$ and $^{187}Os/^{188}Os$, and others (e.g. Cohen & O'Nions, 1982; Allegre *et al*., 1987; Hart *et al*., 1992). Another set of observations is provided by seismic tomography, which shows that gigantic pieces of the oceanic slabs are stagnated at the 660 km discontinuity (e.g. van der Hilst *et al*., 1997), and some of them are subducted even deeper into the lower mantle to a depth of ~1500–2700 km (e.g. van der Voo *et al*., 1999). The possibility of subduction of crustal materials into the lower mantle is also justified by experimental data based on comparison of the densities and viscosities of mantle and crustal minerals synthesized at extremely high pressures and temperatures (e.g. Irifune *et al*., 1994; Yagi *et al*., 1994; Nishiyama *et al*., 2005).

In recent years, because of progress in UHP experimental technologies, many new minerals have been synthesized at 6–20 and >20 GPa in the KNASH, KASH, and ASH chemical systems (e.g., wadeite, topaz-OH, phase egg, K- and Na-hollandite, stishovite, and others), but none of these minerals (except topaz-OH) has yet been identified within natural UHPM terranes. A survey of the available literature shows that 'hunting' for deeply subducted natural rocks is growing rapidly and that the 'traces' of the deep subduction recorded in natural rocks can be successfully understood through the mutual observations of mineral chemistry, crystal structure, microstructural topology of nanometric inclusions, and the microtextural features of metamorphic mineral assemblages (e.g. van Roermund & Drury, 1998; Bozhilov *et al*., 1999; Dobrzhinetskaya *et al*., 2004, 2005, 2006; Spengler *et al*., 2006). Most experiments carried out on reproduction of mineralogy of continental crust at 6–20 and >20 GPa are performed with the starting materials such as gels, glasses, or sintered chemical oxides, with a bulk chemistry corresponding to standard pelagic or terrigenous sediments, and/or standard average continental crust. Such starting materials are used to speed kinetics and to easily establish chemical equilibrium. However, the possible microstructural and textural transformations, which might occur as a result of breakdown of the previous minerals and the appearance of newly grown minerals, would be definitely missed in such experiments. Although chemically 'averaged' starting material provides rapid results for general understanding of the fate of continental crust during its deep subduction, the diverse compositional range of continental crust lithologies that have been involved in UHPM events has yet to be explored.

We describe here the results of experimental studies of UHPM assemblages in two different bulk compositions corresponding to Na-rich granite from the Kokchetav massif, Kazakhstan, and felsic gneisses from Erzgebirge, Germany; both are classic UHP diamond-bearing terranes. The starting materials are intentionally composed of natural mineral mix thus allowing us to observe some microstructural–textural features of the breakdown or dehydration of starting minerals, followed by their replacement with high-pressure phases equilibrated at 9–12 GPa at 1000–1300 °C.

EXPERIMENTAL PROCEDURES

Starting materials

Two starting materials, mixes A and B, using powdered to ≤5 μm natural minerals (Wards, Inc.) were prepared. To measure average bulk chemistry, the mineral mix powder was placed into a Pt crucible and melted at 1500 °C at ambient pressure for 3 h. The melt was quenched to 450 °C for 30 min and cooled to room temperature for 4 h. No minute minerals were found in these glasses with scanning electron microscope (SEM) imaging performed in back-scattered electron mode. The glass product was mechanically broken into small fragments (0.1–0.3 mm), which were mounted on the holder, coated with graphite film, and measured by an electron microprobe (EMP) equipped with wavelength dispersive spectrometers (WDS).

Mix A consists of (vol.%) plagioclase–$NaAlSi_3O_8$ (45), microcline (15), quartz (25), and biotite (15). Several flaky fragments of biotite (size of 50–100 μm) were added to the powdered material to produce microstructural patterns of biotite breakdown and dehydration at high pressures. The average bulk chemistry of mix A was (in wt%): $SiO_2 = 68.20$; $Al_2O_3 = 13.03$; $FeO = 1.20$; $TiO_2 = 1.05$; $MgO = 1.0$; $CaO = 3.0$; $Na_2O = 5.60$; $K_2O = 4.5$; sum = 97.58.

Mix B contains (vol.%) plagioclase (oligoclase with albite lamellae) (45), microcline (12), quartz (16), garnet-almandine (10), phengite (13), kyanite (2.5) and rutile (0.5). The average bulk chemistry of mix B was (wt%): $SiO_2 = 64.80$; $TiO_2 = 0.86$; $Al_2O_3 = 17.20$; $FeO = 4.12$; $MnO = 0.03$; $MgO = 1.82$; $CaO = 1.72$; $Na_2O = 2.33$; $K_2O = 4.05$; sum = 96.93.

The starting powder was loaded into a Pt container, which was arc-welded from both ends. Positive control of oxygen fugacity was obtained by placing Ni-foil into the Pt container at one end of the starting material. The Ni reacts with free interstitial oxygen, producing NiO, and, therefore, buffers fO_2 at a level of about −4 log units (e.g. Eggler & Baker, 1982).

Apparatus and procedure

Experiments were performed with a Walker-style multianvil apparatus using as a sample temperature–pres-

sure media a 6-mm truncated edge length (TEL) semi-sintered MgO-Al_2O_3 octahedron prepared from powdered ceramic material (584-OS) provided by Aremco Products, Inc. Two rolls of Rhenium-foil of 0.0254 mm thickness were used as a heater, and arc-welded Pt capsules served as a container for starting material. Spaces between the Rhenium heater, the thermocouples, and the Pt container were filled with the semi-sintered MgO tuber, disks, and MgO powder similar to what has been described elsewhere in detail (Dobrzhinetskaya *et al.*, 2005). Other materials and small devices placed within the internal part of the multianvil apparatus pressure chamber included eight tungsten carbide (WC) 25-mm cubes, each with a 6-mm truncation on one corner, and sheets of fibreglass laminate (G-10) coated with Dry Film Vydax Mold Release, which were placed between the eight WC cubes and the six anvils. Desirable pressure was pumped automatically at a speed of 150 r.p.m., and maintained constant using an Omega controller setup. Temperature, measured with D-type thermocouples (W3%Re–W25%Re), was increased manually with a speed $\sim$20 °C min^{-1}, and it was maintained constant to within $\pm$ 3 °C using an automatic 832 Eurotherm controller. No temperature corrections for the effect of pressure on the thermocouple's emf were performed. The 6-mm TEL assembly was calibrated at high temperature, establishing a coesite-to-stishovite transition at 9.3 GPa and 1200 °C, and Mg_2SiO_4 alpha to beta transition at 14.5 GPa and 1400 °C. The total uncertainty in pressure was $<$0.1 GPa. The temperature distribution within the sample was calculated using the empirical equation of O'Neill & Wood (1979), established on the basis of experimental studies of Fe-Mg partitioning between garnet and olivine. We have known from such a calibration that the real temperature in the central part of the samples is $\sim$50 °C higher than that read by the thermocouple. Experimental temperatures shown in Table 1 were corrected in this way.

Experimental conditions and methods of studies

Experiments were performed at 9–12 GPa and 1000–1300 °C, and lasted from 5 to 46 h (Table 1). Each experiment was quenched in seconds to 90–110 °C by shutting off the power to the apparatus, followed by automatic depressurization to atmospheric pressure at a speed of $-$0.5 GPa h^{-1}.

After recovery from the apparatus, samples were cut longitudinally into two pieces, and polished sections were prepared for study of the mineral assemblies with the aid of an optical microscope (polarized light), an EMP, an SEM, laser micro-Raman spectroscopy, and X-ray diffraction methods (Tables 2–4).

Electron microprobe analyses were performed with a JEOL JXA-8900 Super Probe (Waseda University, Tokyo, Japan) using the wavelength dispersive method and an LaB6 filament. The measurements were performed at a 15 kV accelerating voltage, with a 20 nA beam current, a 2 μm beam size, and a counting time interval of 10 s. The data were corrected using the ϕ-ρ-Z method (JEOL Ltd, 1993).

Scanning electron microscopy and energy-dispersive X-ray microanalysis (EDAX) were performed at the Central Facility for Advanced Microscopy and Microanalysis at the University of California at Riverside, CA, USA, with a Philips XL30 instrument equipped with field emission gun, operated at 15 kV. The EDAX microanalytical system of the microscope includes an energy-dispersive spectrometer (EDS) equipped with an Si detector with a super-ultrathin window with a resolution of 137 eV at MnKα. The spectral data were acquired at 1500–2000 counts s^{-1} with dead time below 25%, a beam current of 1 nA, an effective spot size of $\sim$1.5–2 μm, and a 40 s counting time; they were corrected using the eDXi software from EDAX and the ZAF correction scheme (Armstrong, 1988).

Laser Raman spectroscopy was performed using a Jobin Yvon Horiba Raman microscope (Waseda University, Tokyo, Japan), with the CCD4 detector at excitation line 514.527. We used objective lenses $\times$100; spectra were accumulated during 10 s with the beam diameter as small as 2 μm.

X-ray diffraction data were collected directly from the polished samples with the aid of a Rigaku D/Max 2000/PC micro-diffractometer equipped with the SmartLab software system (Rigaku Inc.). Counting time was 3 axes/2800 s, and the beam diameter was $\sim$100 μm. Standard D-spacing of minerals was obtained from Rigaku's archive database.

RESULTS

Starting material of mix A

One reconnaissance experiment was conducted with mix A bulk chemistry to understand if $KAlSi_3O_8$ and $NaAlSi_3O_8$ can exist as a solid solution of K-Na-hollandite at high pressure and temperature, and to ob-

Table 1. Experimental conditions and results. Asterisk identifies experiment number for which starting material was mix A. Mix B was used as starting material for experiments without the asterisk.

Run number	P (GPa)	T (°C)	t (h)	Run products
ma215a*	12	1300	46	grt, cpx, stish, K-Na-hol, K-rich mica with unknown structure, fluid
ma215b	12	1300	46	grt, cpx, stish, K-Na-hol, topaz-OH, rutile with α-PbO_2 structure, melt
ma293	12	1100	24	grt, cpx, stish, K-Na-hol, topaz-OH, rutile with α-PbO_2 structure
ma294a	10	1100	18	grt, cpx, stish, K-Na-hol, topaz-OH, rutile with α-PbO_2 structure
ma295	10	1000	5	grt, cpx, stish, K-Na-hol, pheng, ky
ma297	9	1200	24	grt, cpx, coes, K-Na-hol, ky, rutile with α-PbO_2 structure, melt

grt, garnet; cpx, clinopyroxene; stish, stishovite; K-Na-hol, K-Na-hollandite; pheng, phengite; ky, kyanite.

Table 2. Electron microprobe wavelength dispersive spectrometer (WDS) and energy-dispersive spectrometer (EDS) analyses of run products. EDS analyses are normalized to 100.

Oxides, wt%										
SiO_2	TiO_2	Al_2O_3	MgO	MnO	CaO	FeO	K_2O	Na_2O	Cr_2O_3	Sum
ma215a $P = 12$ GPa, $T = 1300$ °C										
Jadeite (4) $X_{jd} = 0.99$										
59.35	0.00	23.75	0.00	0.00	0.70	0.30	0.00	16.14	0.00	100.24
Porphyroblastic stishovite (3)										
95.60	0.30	1.75	0.00	0.00	0.00	0.15	0.00	0.00	0.00	97.80
Garnet from myrmekites (3) Si = 3.12 cpfu										
42.05	0.12	21.31	12.65	0.00	5.10	16.78	0.10	1.20	0.00	99.31
K-mica with unknown structure (3)										
45.25	2.30	14.10	14.30	0.00	0.00	17.80	3.95	2.30	0.00	100
K-Na-hollandite (3)										
65.01	0.00	18.2 8	0.00	0.00	0.00	0.00	15.57	1.20	0.00	100.03
ma215b $P = 12$ GPa, $T = 1300$ °C										
Jadeite (3) $X_{jd} = 0.99$										
58.20	0.03	25.60	0.09	0.00	0.58	0.45	0.00	15.20	0.00	100.15
Garnet (5) Si = 3.14 cpfu										
41.63	0.07	20.19	12.06	0.00	4.90	19.24	0.00	0.34	0.00	98.78
Stishovite (2)										
95.40	0.05	2.03	0.00	0.00	0.00	0.35	0.00	0.00	0.00	98.28
K-Na-hollandite (5)										
65.05	0.00	17.30	0.00	0.00	0.00	0.00	16.29	1.41	0.00	100.05
Topaz-OH(5)										
35.13	0.26	54.19	0.07	0.02	0.04	0.69	0.00	0.00	0.04	90.44
ma293 $P = 12$ GPa, $T = 1100$ °C										
Jadeite(2) $X_{jd} = 0.98$										
58.16	0.08	24.03	0.38	0.00	0.59	1.18	0.00	14.83	0.05	99.30
Garnet (2) Si = 3.14 cpfu										
41.97	0.12	21.05	12.55	0.00	5.02	17.43	0.00	0.38	0.09	98.61
Stishovite (2)										
97.40	0.12	1.40	0.00	0.00	0.00	0.20	0.00	0.00	0.00	99.12
K-Na-hollandite (5)										
65.47	0.00	17.64	0.00	0.00	0.00	0.20	15.63	1.32	0.30	100.56
Topaz-OH(5)										
35.64	0.17	56.87	0.05	0.00	0.02	0.67	0.00	0.01	0.07	93.20
ma294a $P = 10$ GPa, $T = 1100$ °C										
Jadeite(2) $X_{jd} = 0.97$										
59.10	0.12	22.90	0.10	0.08	0.72	1.30	0.00	14.70	0.10	99.12
Garnet (2) Si = 3.05 cpfu										
40.15	0.16	21.02	12.04	0.00	4.47	20.43	0.00	0.50	0.09	98.8 6
Stishovite (2)										
98.00	0.00	1.10	0.00	0.00	0.00	0.30	0.00	0.00	0.00	99.40
K-Na-hollandite (3)										
65.50	0.00	18.1 2	0.00	0.00	0.00	0.30	15.23	1.25	0.12	100.52
Topaz-OH(3)										
33.69	0.22	56.96	0.05	0.00	0.05	0.65	0.01	0.00	0.00	90.63
ma295 $P = 10$ GPa, $T = 1000$ °C										
Jadeite (3) $X_{jd} = 0.94$										
57.90	0.10	24.60	0.18	0.00	0.72	1.68	0.00	14.20	0.00	99.38
Garnet (2) Si = 3.04 cpfu										
40.5 2	0.10	21.78	11.48	0.00	5.13	20.49	0.00	0.3 8	0.00	99.88
Stishovite (2)										
98.40	0.09	0.82	0.00	0.00	0.00	0.08	0.00	0.00	0.00	99.39
K-Na-hollandite (3)										
65.87	0.00	19.22	0.00	0.00	0.00	0.31	14.10	0.58	0.00	100.08
Phengite (3)										
60.01	1.29	23.47	0.56	0.29	0.00	0.36	11.60	0.12	0.00	97.70
ma297 $P = 9$ GPa, $T = 1200$ °C										
Jadeite (3) $X_{jd} = 0.93$										
59.60	0.09	22.60	0.20	0.00	1.72	1.90	0.00	14.20	0.00	100.31
Garnet (2) Si = 3.01 cpfu										
40.00	0.60	22.78	12.30	0.00	4.02	18.47	0.00	0.23	0.00	98.40
Coesite (2)										
99.02	0.00	0.00	0.00	0.00	0.00	0.00	0.00	0.00	0.00	99.02
K-Na-hollandite (3)										
65.01	0.00	18.20	0.00	0.00	0.00	0.21	14.60	0.48	0.00	99.59
Topaz-OH (2)										
35.38	0.18	54.78	0.07	0.00	0.04	0.53	0.00	0.00	0.07	91.05

Numbers of chemical analyses are given in parentheses.

serve the character of the breakdown reaction of biotite, a potential source of fluid. The run product (ma215 a) of sodium-rich granite held for 46 h at 12 GPa and 1300 °C was completely recrystallized. It consisted of jadeite (jd), K-Na-hollandite (K-Na-hol), stishovite (stish), garnet (grt) and a K-mica phase of

Table 3. Well-defined Raman peaks (cm^{-1}) of run products.

Stishovite (8) ma215a,b	Coesite (4) ma297	Rutile with α-PbO_2 structure (6) ma215b	K-Na-hollandite (10) ma215b, 297	Jadeite (5) ma215a,b	Topaz-OH (7) ma215b, 294, 293
				985.9–990.6	924.2–930.4
758.3–760.2			**764.4–765.2**	**697.4–701.2**	
			623.7–625		
586.9–589.2	**521.6–524.4**			572.4–574	
		424.5–428.9			456.4–459.8
	333.3–353.4	355.2–352.1		375.3–379.2	334.6–338.9
		311.8–314.2			
	271.7–274.5	283.7–283.9	275.9–273.0		**268.6–269.8**
231.2–238.6			209.2–211.0		
	172.80–180.39	172.5–174.0			

Bold numbers correspond to the diagnostic peaks. Number in parentheses corresponds to the number of examined minerals.

Table 4. D-spacing in Å (micro X-ray diffraction data).

Stish standard	Stish ma215a Spot 1	Stish ma215b Spot 1	Topaz-OH standard	Topaz-OH ma215b Spot 1	Topaz-OH ma215b Spot 2	K-hol standard	K-Na-hol ma215a Spot 1	K-Na-hol ma215a Spot 2
2.9582	2.9555	2.9441	2.9370	2.9341	1.8661	2.1800	2.1875	1.7559
2.2487	2.2465	2.2543	1.9340	1.9302	1.6061	1.8220	1.8254	1.5499
2.0904	2.0778	2.0796	1.8691	1.8618	1.5681	1.7580	1.7559	1.5276
1.9806	1.9746	1.9730	1.6014	1.6050		1.6120	1.6195	1.3697
1.4778	1.4751	1.4724	1.5684	1.5691		1.5630	1.5650	1.3599
1.3330	1.4734	1.3317				1.5400	1.5494	1.3558
1.2927	1.3310	1.2817				1.5270	1.5249	
	1.2805					1.3810	1.3818	
						1.3660	1.3676	
						1.3600	1.3590	
						1.3530	1.3572	

unknown structure. Jadeite, at 35% in volume, was the most abundant phase in this experiment, which, together with stishovite, formed fine-grained aggregates (Fig. 1a,b). As no chemical analyses were obtained because of small grain size, jadeite and stishovite were confirmed with Raman spectroscopy (Table 3) due to the presence of well-developed peaks at 697.4–701.2 cm^{-1} (jd) and high-intensity sharp peaks at 586.9–589.2 cm^{-1} (stish). There were also porphyroblastic (20–30 μm in size) tabular or elongated crystals of stishovite (Fig. 1a–c). They are characterized by sharp high-intensity Raman shifts at 588–589 cm^{-1} and additional lower intensity shifts at 765.8–760.5 and 236.4–238 cm^{-1}. Our interpretation is that the fine-grain aggregates of jadeite and stishovite formed as a result of following reaction:

$$\text{albite} \rightarrow \text{jadeite} + \text{stishovite} \quad (1)$$

Porphyroblastic stishovite is a result of direct, high-pressure transformation of starting grains of quartz to stishovite:

$$\text{quartz} \rightarrow \text{stishovite} \quad (2)$$

K-Na-hollandite ($K,NaAlSi_3O_8$) forms tabular crystals (10–20 μm), which are intergrown together with stishovite (Fig. 1a–c). Micro-X-ray diffraction spectra acquired from tabular crystals of $K_2NaAlSi_3O_8$ yielded the following D-spacing (in Å): 1.7559, 1.5499, 1.5276, 1.3697, 1.3599 and 1.3558, which fit to the standard D-spacing of K-hollandite structure (Table 4). No traces were observed of any intermediate reactions that would be responsible for the transformation of $KAlSi_3O_8$–microcline into $KAlSi_3O_8$–hollandite; therefore, we assume that microcline was transformed into K-hollandite by direct structural transformation:

$$KAlSi_3O_8 - \text{microcline} \rightarrow KAlSi_3O_8 - \text{hollandite}. \quad (3)$$

A small amount of $NaAlSi_3O_8$ was dissolved into porphyroblastic $KAlSi_3O_8$–hollandite, which is indicated by the presence of 1.2 wt% of Na_2O (Table 2) in average chemical analyses (standard deviation is 0.02) summarized from three crystals. As the microstructure shows that K-Na-hollandite is always associated with jadeite and stishovite (Fig. 1a) we propose that structural transformations were accompanied by dissolution of Na-hollandite into K-hollandite according to the reaction:

$$NaAlSi_3O_8 - \text{albite} + KAlSi_3O_8 - \text{microcline} \rightarrow \text{K-Na hollandite} + \text{jadeite} + \text{stishovite}. \quad (4)$$

Finer-grained aggregates of garnet and K-mica of unknown structure compose local domains, which can be easily observed in secondary electron mode of the SEM for their bright contrast and almost classical myrmekitic microstructure (Fig. 1c,d). Myrmekite is a traditional petrographic term, which is used to characterize the symplectitic intergrowth of quartz and

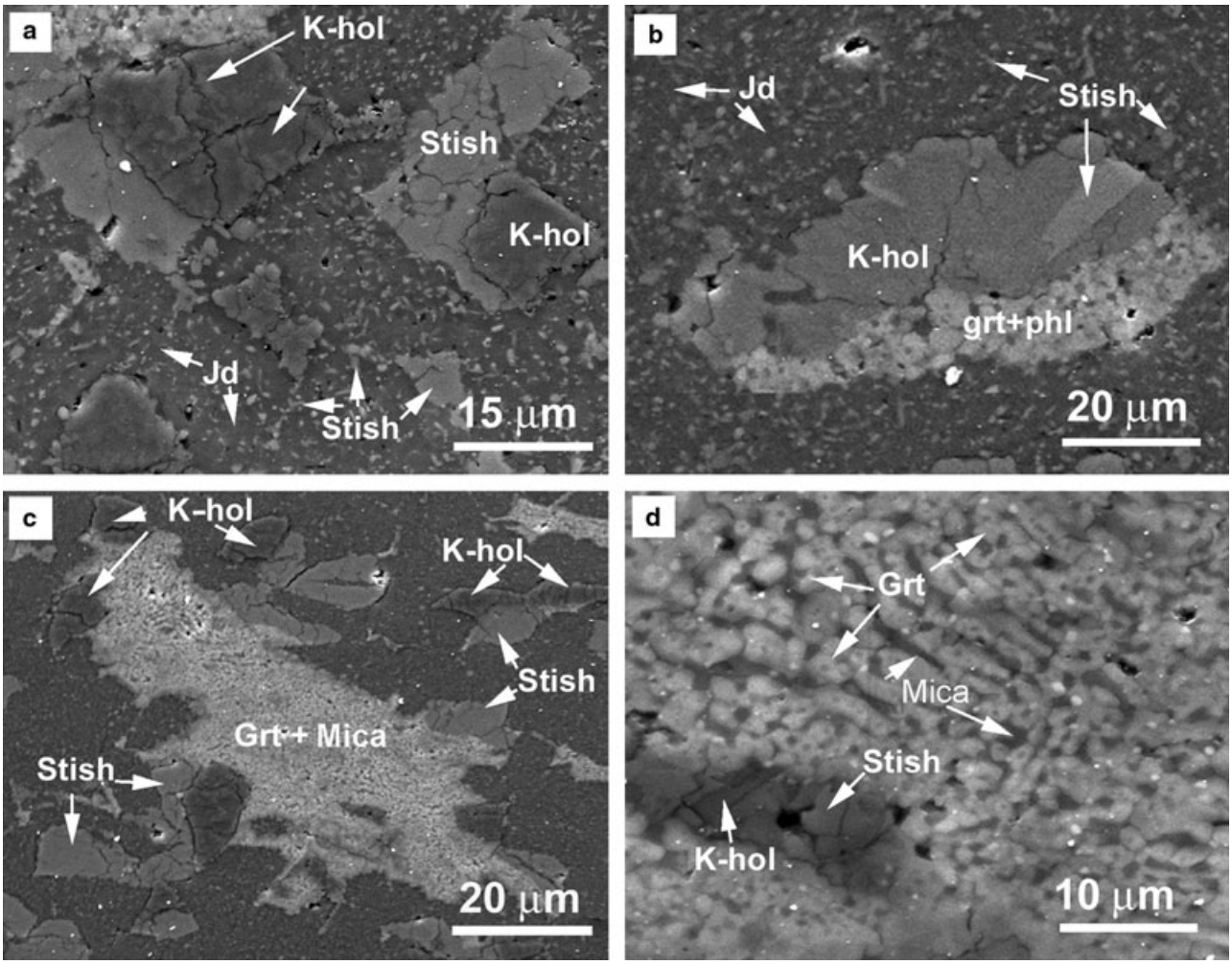

Fig. 1. Secondary electron images of run products ma215a (12 GPa, 1300 °C). Minerals are: K-hol, $K,NaAlSi_3O_8$-hollandite; Jd, jadeite; Stish, SiO_2-stishovite; Grt, garnet; Mica, disordered cation-deficient phlogopite.

plagioclase, or the symplectitic intergrowth of any other minerals that are often developed in regular magmatic and metamorphic rocks of granitoid compositions and in metabasites (e.g. Phillips, 1974; Vernon, 1978; Cesare *et al.*, 2002). Although Fig. 1b shows that garnet + mica myrmekites are situated at the contact with K-hollandite and stishovite intergrowth, another image (Fig. 1c) clearly demonstrates that the myrmekites have replaced former biotite flakes, which was added to the starting material. The following reaction is assumed:

$$\text{biotite} \rightarrow \text{garnet (with majoritic component)} + \text{K-mica} + \text{fluid}. \quad (5)$$

Garnet from myrmekites is non-stoichiometric; average content of Si = 3.12 cations per formula unit (cpfu) (Table 2). Because of the very small size, no representative EMP analyses were obtained with the WDS method from the mica myrmekite component, and therefore an EDS spectrum (Fig. 2) obtained with an SEM is presented here. The spectrum shows the presence of O, Si, Mg, Al, Fe, K, and a small amount of Na and Ti. Semi-quantitative standardless calculations of the oxides obtained with the aid of the EDAX software show that this phase contains ~4 wt% K_2O (Table 2). The cation proportion of the symplectitic mica roughly fits to an interlayer cation-deficient mica, described earlier in Sulu garnet peridotite (Bozhilov *et al.*, 2003b). This is not a conclusive definition, and more precise measurements with the aid of analytical transmission electron microscopy are required. However, it is clear that the cation proportions in the K-mica phase do not fit with phlogopite. The absence of phlogopite in this run is in agreement with the experimental data showing that phlogopite is stable below 9–10 GPa at 1400 °C (Luth, 1997) or below 8–12 GPa at 1250–1350 °C in peridotite assemblages (Harlow, 2002); above these temperature and pressure ranges either K-amphibole or liquid is more stable (Harlow & Davis, 2004).

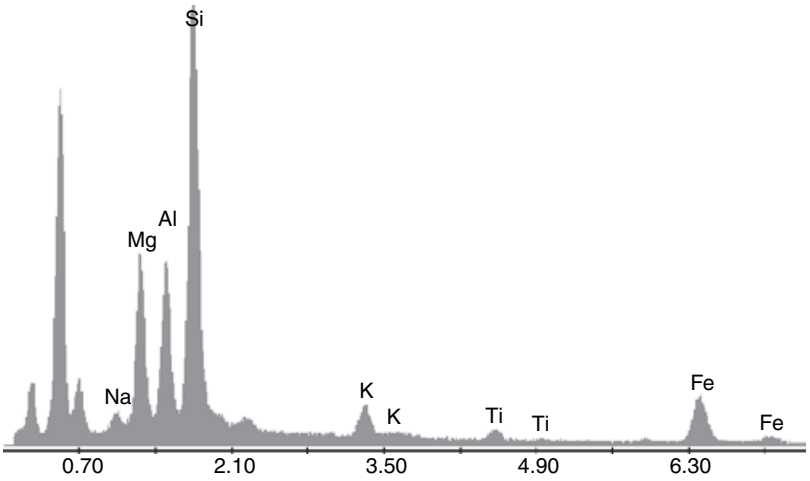

Fig. 2. Energy-dispersive X-ray microanalysis spectrum of mica (disordered cation-deficient phlogopite) from run ma215a (12 GPa, 1300 °C).

Starting material of mix B

Five experiments were conducted using mix B as the starting material at 9–12 GPa and 1000–1300 °C. At 12 GPa and 1300 °C, the run product (ma215b) mineral assemblage consists of garnet, clinopyroxene, K-Na-hollandite, stishovite, topaz-OH, and minor crystals of TiO_2 (Table 1). Garnet of 10–40 μm in size (Fig. 3a,c) is non-stoichiometric, rich in pyrope (average: $X_{alm} = 0.40$, $X_{pyr} = 0.46$ and $X_{grs} = 0.14$), and contains a majoritic component with an average value of Si = 3.14 cpfu (Table 2). Clinopyroxene of 10–20 μm in size (Fig. 3a,c) is represented by almost pure sodic pyroxene ($X_{jd} = 0.99$). K-hollandite is characterized by 10–30 μm-size grains (Fig. 3b,c). Its chemical composition shows the presence of $KAlSi_3O_8$-$NaAlSi_3O_8$ solid solution ($Na_2O = 1.41$ wt%) (Table 2). Hollandite structure is confirmed by Raman spectroscopy: the diagnostic peaks at 764–765.2 cm^{-1} and other peaks at 623.7–625, 275.9–273.0 and 211–209.2 cm^{-1} correspond to standard K-hollandite (Table 3). Stishovite forms elongated prismatic or tabular crystals of different sizes (5–20 μm), and it contains ~2 wt% of Al_2O_3. The presence of some H^+ is also expected because WDS analyses of stishovite are < 100 % (Table 2). The stishovite structure of SiO_2 in this run product is confirmed by Raman shifts at 586.9–589.2 cm^{-1} (Table 3).

Topaz-OH is also widely developed in this run product (Fig. 3a), and it forms isometric crystals of 10–30 μm size with some of them containing tiny inclusions of kyanite. The latter suggests that the topaz-OH crystals were formed as a result of reaction of kyanite and water. Topaz-OH contains 9.56 wt% H_2O, and no fluorine was detected. The topaz-OH structure is confirmed with Raman spectroscopy from the presence of high-intensity diagnostic peaks at 268.6–269.8 cm^{-1}, and others developed at 924.2–930.4, 456.4–459.8, and 334.6–338.9 cm^{-1} (Table 3). The D-spacing obtained with the aid of X-ray diffraction also fit with those obtained from standard topaz-OH (Table 4). A few grains of rutile (Fig. 3a,c) with a α-PbO_2 structure were identified by Raman spectroscopy due to the presence of diagnostic peaks at 424.5–428.9 cm^{-1} and well-developed, sharp peaks at 355.2–352.1, 311.8–314.2, 283.7–283.9 and 172.5–174.0 cm^{-1}. Poikilitic domains contain symplectites, which consist of a mixture of small crystals (< 2 μm) of garnet, K-Na-hollandite, stishovite, topaz-OH, TiO_2 with α-PbO_2 structure, and a small amount of glass (Fig. 3d). This mineral association was probably formed as result of phengite dehydration, although crystallization from a partial melt cannot be excluded. The following reactions, which might be responsible for the mineral assemblage, are consistent with our experimental results at 1300 °C and 12 GPa:

$$\text{phengite} = \text{garnet} + \text{K-Na-hollandite} + \text{stishovite} + H_2O, \quad (6)$$

$$\text{kyanite} + H_2O = \text{topaz-OH}, \quad (7)$$

$$\text{rutile} \rightarrow TiO_2 \text{ with } \alpha\text{-}PbO_2 \text{ structure}. \quad (8)$$

At pressures of 12 and 10 GPa and the same temperature of 1100 °C (ma293 & ma294a), no phengite was left in the run product; instead garnet was observed in association with K-hollandite, topaz-OH, stishovite, and TiO_2. Garnet contains Si = 3.09 cpfu at 12 GPa, and its majoritic component slightly decreases with decreasing pressure: Si = 3.05 cpfu at 10 GPa. Clinopyroxene is almost pure jadeite (Table 2).

The experiment conducted at 10 GPa and 1000 °C (ma295) lasted only 5 h due to the failure of the thermocouple; it was quenched at that time rather than accept possible unknown changes of temperature. Although the garnet exhibited compositional zoning, indicating that complete recrystallization of garnet was not reached, all starting plagioclase was completely replaced by a new mineral assemblage. The zoned

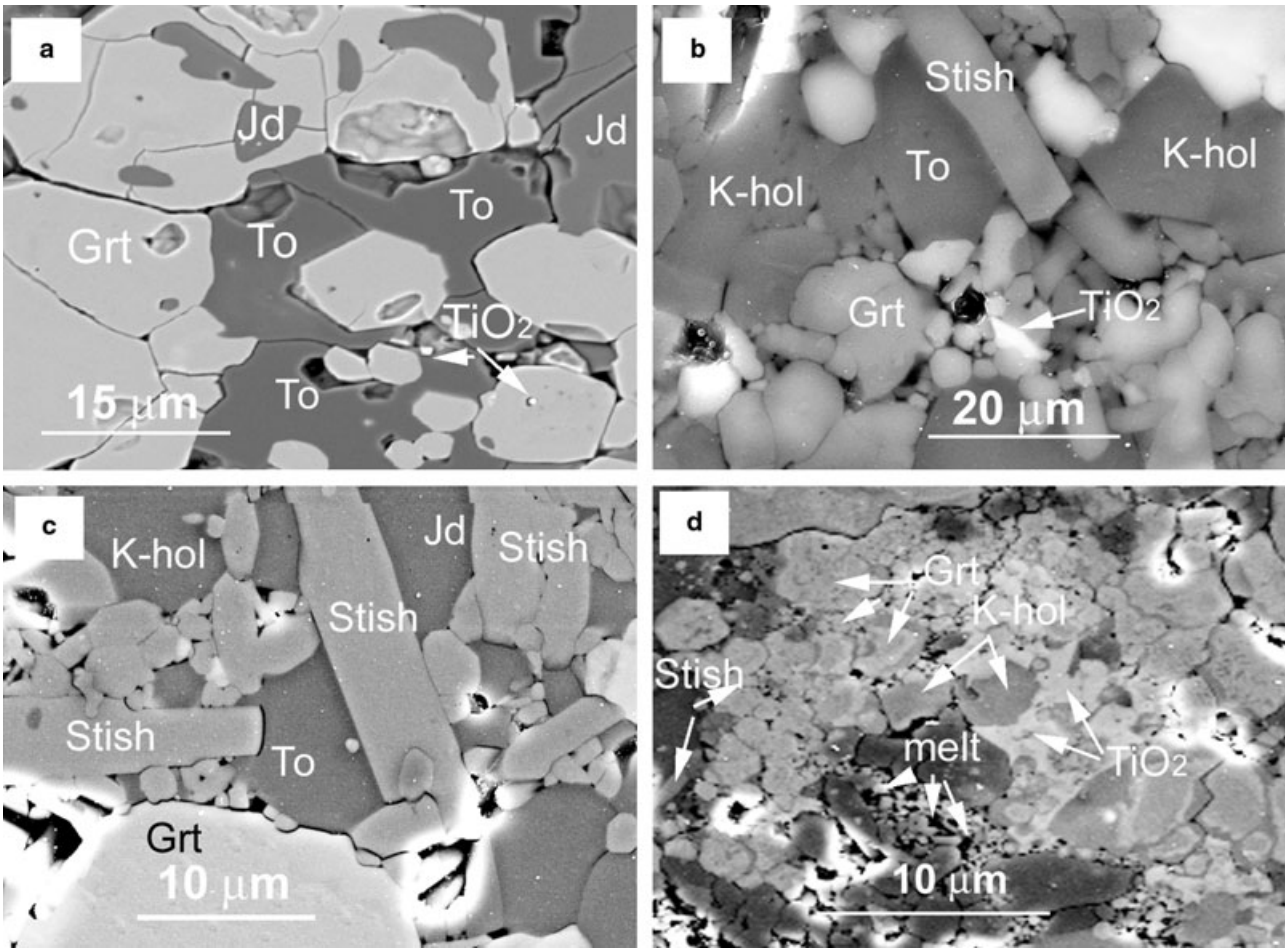

Fig. 3. Secondary electron images of run products ma215b (12 GPa, 1300 °C). To, topaz-OH; other mineral abbreviations are as Fig. 1.

garnet coexists with clinopyroxene ($X_{jd} = 0.94$), K-Na-hollandite, stishovite, phengite and kyanite. The rim of garnet contains Si = 3.04 cpfu, whereas the core composition remains close to the starting garnet (Si = 2.98 cpfu). No topaz-OH was found in this run product, although, formally, the *P–T* conditions of the experiment corresponded to the topaz-OH stability field (e.g. Wunder *et al.*, 1993, 1999; Schmidt *et al.*, 1998; Ono, 1999; Sano *et al.*, 2004). We believe that topaz-OH was not crystallized in this run because phengite is still stable at the given *P–T*; therefore, no fluid was liberated into the system to produce topaz-OH. Another possibility might be the short duration (5 h) of the experiment, which may not have been enough time to cause dehydration of phengite at the given *P–T*. At lower pressure, 9 GPa, and a temperature of 1200 °C (ma297), coesite was crystallized instead of stishovite in association with garnet, clinopyroxene, K-hollandite, kyanite, and rutile with α-PbO_2 structure. Coesite was confirmed with Raman spectroscopy: peaks of (cm^{-1}) 521.6–524.40, 333.30–353.40, 271.70–274.50, and 172.80–180.39 (Table 3). A standard coesite Raman shift at 521 cm^{-1} was observed. Although the lower wavelength number shift at 172.8–180.39 cm^{-1} is overlapped by that of rutile, with α-PbO_2 structure (172.5–174.0 cm^{-1}), the presence of 521.6–524.40 cm^{-1} leaves no doubt of the coesite structure. A small amount of melt was also produced in this run: minute crystals of kyanite and K-Na-hollandite were observed within amorphous domains of glass. No topaz-OH was identified in the ma297 run product.

Variation of mineral proportions in run products as a function of pressures

It is known from previous studies that the volume proportion of minerals in synthetic rocks of 'continental crust' or 'continental sediments' bulk chemistry is a function of pressure (e.g. Irifune *et al.*, 1994; Domanik & Holloway, 1996; Ono, 1998; Nishiyama *et al.*, 2005). The variation in mineral proportions is remarkable in the pressure range from 6 to $\geqslant$15 GPa. At ~8 to 10–11 GPa, phengite breaks

down, and liberated water reacts with kyanite producing topaz-OH (see Eqs 6 & 7). The $KAlSi_3O_8$-hollandite becomes stable above 8–9 GPa (e.g. Yagi *et al.*, 1994). In our experiments $KAlSi_3O_8$-$NaAlSi_3O_8$-hollandite solid solution was synthesized at 12 GPa and 1300 °C, pure $KAlSi_3O_8$ end member was also observed. Above ~12 GPa, topaz-OH no longer exists. It will be replaced by the phase egg [$AlSiO_3(OH)$], which is stable to pressures of more than 20 GPa (e.g. Sano *et al.*, 2004) (Fig. 4). In our experiments, which fall in the range of 9–12 GPa, the variation of mineral proportions is not very strong. With increasing pressure, garnet in the experiments became more majoritic, with a tendency to increase the Si from 3.01 cpfu at 9 GPa to 3.14 cpfu at 12 GPa. At the same time, Al content in garnet decreases, whereas coexisting clinopyroxene becomes Al-rich: $X_{jd} = 0.93$ at 9 GPa and $X_{jd} = 0.98$–0.99 at 12 GPa. Because of such changes in compositions, the modal proportion of garnet in the run products increases with increasing pressure because part of clinopyroxene dissolves into garnet. The modal fraction of garnet in our experiments varied from 25 to 27 vol.% at 9 GPa to 30–32 vol.% at 12 GPa. The amount of clinopyroxene decreased respectively from ~15–16 vol.% at 9 GPa to 10–12 vol.% at 12 GPa, although in Na-rich starting material (mix A) ~35% jadeite was found at 12 GPa. The transition from coesite to stishovite did not exhibit any visible changes in modal fraction at the given pressure ranges. It is worth pointing out that our experiments are not reversed, and therefore, kinetics effects might play an important role in the modal amounts and minerals chemistry.

Comparison of experiments with previous studies

The presence of high-pressure polymorphs of SiO_2 (stishovite and coesite) in all the experiments (both mixs A and B) is in good agreement with the coesite–stishovite stability boundary established by Zhang *et al.* (1996). No topaz-OH was produced in mix A, probably because the system was not rich enough in Al and H_2O. Topaz-OH was crystallized in three of the five experiments with mix B at 12 and 10 GPa, where no phengite and kyanite were left, and this is consistent with the topaz-OH-stishovite stability field established by many experiments carried out in different laboratories (Wunder *et al.*, 1993, 1999; Schmidt *et al.*, 1998; Ono, 1999; Sano *et al.*, 2004) (Fig. 4). The absence of topaz-OH in run ma297 at 9 GPa and 1200 °C is also consistent with the data mentioned above plotted on a *P–T* diagram of Al-rich phases (Fig. 4). However, there is an inconsistency with run ma295, which plots inside the topaz-OH stability field (Fig. 4), even though no topaz-OH was identified. This discrepancy is attributed to a short duration of the run (5 h), which probably was not enough to complete reactions shown as Eqs (6) and (7). This interpretation is also supported by the presence of both phengite and kyanite in ma295 run product (Table 1).

With regard to the KNAMCFS system, which is close to the real UHPM rock compositions, a few studies have been performed at the pressure range of 9–12 GPa. Irifune *et al.* (1994) conducted short-time anhydrous experiments (10–130 min) at 6–24 GPa and 1250–1900 °C on average continental crust composition (in wt%: $SiO_2 = 66.0$; $TiO_2 = 0.5$; $Al_2O_3 = 15.2$; FeO = 4.5; MgO = 2.2; CaO = 4.2; $Na_2O = 3.9$; $K_2O = 3.4$)

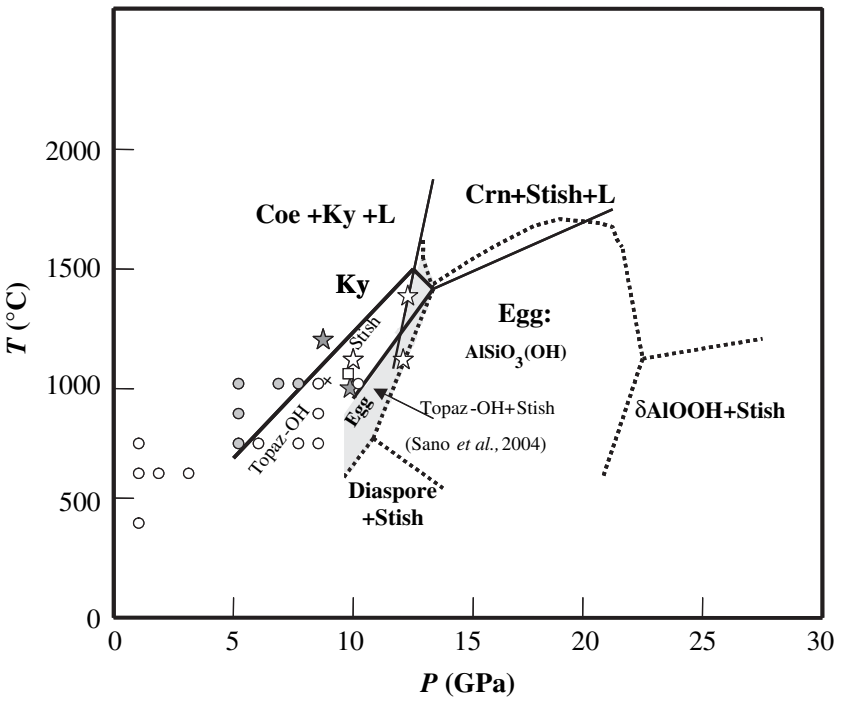

Fig. 4. Summarized *P–T* diagram of topaz-OH [$Al_2SiO_4(OH)_2$] stability field and its relationships with other Al-rich phases. Data are adapted from Ono (1998, 1999), Sano *et al.* (2004) and Wunder *et al.* (1993, 1999). Black lines – stability field of topaz-OH adapted from Ono (1999); dashed black lines – topaz-OH and phase egg [$AlSiO_3(OH)$] stability field adapted from Sano *et al.* (2004); the area filled with grey colour is the field where topaz-OH + stishovite are stable according to Sano *et al.* (2004), this area overlaps the conditions where phase egg is stable instead of topaz-OH and stishovite according to Ono (1998). Data adapted from Wunder *et al.* (1993, 1999): filled (grey) circles – Ky + H_2O, open circles – experiments where topaz-OH was synthesized; square – data from Pawley (1994). Data obtained by Schmidt *et al.* (1998) are not placed on this diagram because their topaz-OH + phase egg stability field partly overlapped the area, which is filled with grey. Our experiments: runs labelled as filled stars contain no topaz-OH, open stars indicate presence of topaz-OH; run215a (mix A) is not plotted because it has different bulk chemistry then other plotted runs. Coe, coesite; Ky, kyainite; Crn, corundum; Stish, stishovite; L, fluid/melt.

adopted from Taylor & McLennan (1985). The chemical compositions of the run products are available only for the experiments performed at 6, 10, 17.5, 21 and 24 GPa in Irifune *et al*. (1994). Although the starting material mix B contained slightly less Si, Ca, Na, but more Al than 'average continental crust,' experiment ma677 conducted by Irifune *et al*. (1994) at 10 GPa, 1200 °C and 1.5 h was chosen for comparison with our run ma294a annealed at 10 GPa, 1100 °C for 18 h. In their run ma677, stishovite contains 2.04 wt% Al_2O_3, whereas in our experiment stishovite had less Al_2O_3 (1.4 wt%), which is explained by the lower temperature. Clinopyroxene is jadeitic in both experiments, but in ma677 the jadeitic component ($X_{jd} = 0.85$) is less than in ma294a ($X_{jd} = 0.97$). Garnet is characterized by almost the same value of the majoritic component in both experiments, i.e. Si = 3.04 cpfu in ma677 and Si = 3.05 cpfu in ma294a. The latter confirms that the experiments are consistent because the majoritic component in garnet is a function of pressure and is almost insensitive to differences in temperature. K-hollandite in ma677 is represented by the pure $KAlSi_3O_8$ end member, whereas in our experiment it contains 1.25 wt% Na_2O, and thus we consider that the K-hollandite in run ma294a represents a solid solution of two components, $KAlSi_3O_8$ and $NaAlSi_3O_8$. Kyanite was produced in ma677, whereas in ma294a topaz-OH was identified. The given mineralogical difference is due to the presence of a water-bearing phase, phengite, in our starting material. No water was introduced into the mix of chemical oxides chosen as a starting material for experiment ma677 (Irifune *et al*., 1994).

Our data were also compared with experiments performed by Ono (1998) who used as the starting material a gel with a bulk chemistry of typical pelite (in wt%: $SiO_2 = 63.4$; $TiO_2 = 0.9$; $Al_2O_3 = 18.0$; FeO = 7; MgO = 2.8; CaO = 2.4; $Na_2O = 1.7$; $K_2O = 3.9$; sum = 100) adopted from Miller (1985). Ono (1998) reported that his starting gel contained 6 wt% H_2O; however, no recalculation of the typical pelitic bulk analysis with respect to added water was provided. In general, the bulk composition of the Ono starting material is comparable with our mix B, although there was more Si and Na, less Fe, Mg and H_2O in the mix, while Al Ca, and K contents were almost the same. Ono (1998) plotted his experimental data on a *P–T* diagram (Fig. 5), and a series of lines were used to separate the diagram into two major fields. The field in the lower part of the diagram outlined the *P–T* conditions at which hydrous phases are stable, and the upper field the conditions where no hydrous phases were synthesized from the same starting material. Our run ma293 containing topaz-OH (12 GPa & 1100 °C) is in good agreement with Ono's data in that it plots on the lower side of the diagram where high-pressure hydrous phases are present. Sample ma293 also plots exactly on the additional sub-boundary that separates topaz-OH and phase egg [$AlSiO_3(OH)$] in run sh16 performed by Ono (1998) under similar conditions. The absence of phase egg in our ma293 experiment may be explained by possible differences in kinetics between our and Ono's starting material. However, it may also be due to existing uncertainties in determination of the boundary which separates the field where

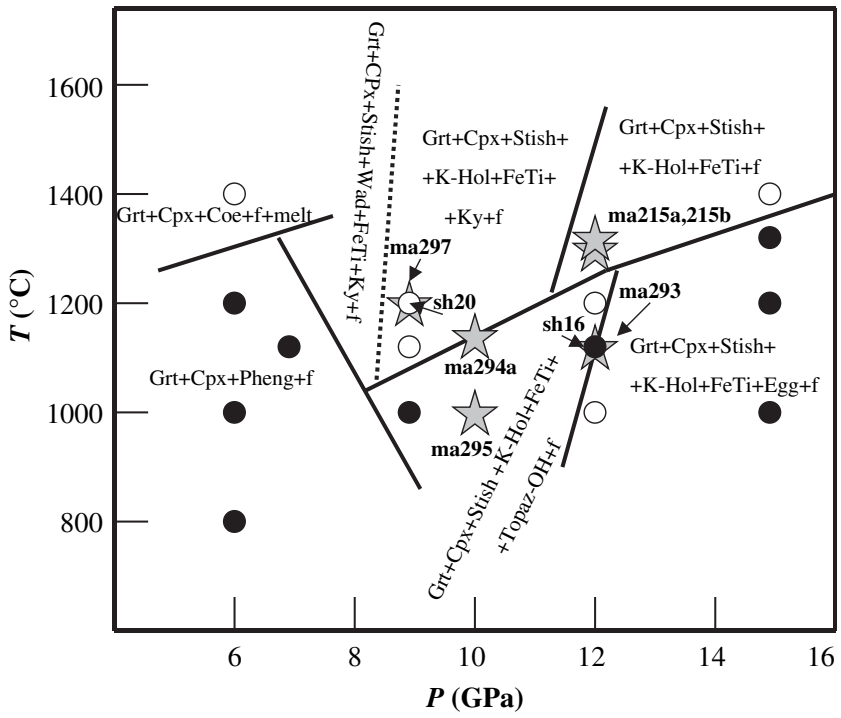

Fig. 5. Experimental data for the typical sediment (pelite) composition adopted from Ono (1998) and our data for comparison plotted onto *P–T* diagram. *P–T* regions containing different phases outlined by solid and dashed lines are from Ono (1998). Solid circles – experiments, where hydrous minerals were produced; open circles – with no hydrous phases (Ono, 1998); filled stars – our data. Mineral abbreviations are as Fig. 4.

topaz-OH + stishovite are stable from the conditions where they are replaced by the egg phase (Fig. 4). Run ma294a containing topaz-OH is considered to be very close to Ono's result (Fig. 5), although the solid line, on which run ma294a is plotted, needs to be shifted to the upper part of the diagram.

There are also discrepancies between our results and those of Ono (1998). The run ma215b containing topaz-OH (12 GPa & 1300 °C) plots in the upper field of the Ono (1998) diagram, where no hydrous phases were present except for fluid in association with grt + cpx + stish + K-hol + FeTi-oxide. Such a discrepancy may be explained by the absence of experiments at conditions similar to those of Ono (1998). Thus the line separating the 'hydrous phases' and 'non-hydrous phases' fields could be shifted to the upper side of the diagram if more experiments at 11, 10 and 9 GPa and 1300 °C were performed. Another inconsistency also exists between our experiment ma297, and sh20 performed by Ono (1998). Both experiments were carried out at 9 GPa and 1200 °C, but coesite was produced here, whereas Ono (1998) recorded stishovite instead. Because the appearance of coesite at 9 GPa and 1200 °C is consistent with the coesite–stishovite transition boundary established by Zhang *et al*. (1996), this disagreement is attributed to a possible inconsistency in calibration of the apparatus.

Although experiment ma295 plots in the hydrous-phase field (Ono, 1998), phengite (but not topaz-OH) was found to be still stable. This might be because the experiment lasted only 5 h, or it could be attributed to the known uncertainties related to the experimental establishment of the phengite stability field. For example, Schmidt (1996) showed that phengite is stable up to 9.5–10 GPa at 750–1050 °C, whereas Domanik & Holloway (1996, 2000) established a broader range of pressures (8–11 GPa) for the same temperatures (750–1050 °C) at which phengite is still stable.

The chemical compositions of minerals synthesized in our and the Ono (1998) experiments are consistent with existing *P–T* conditions, and they are also in good agreement with each other, with few exceptions. For example, stishovite in run ma293 incorporates 1.4 wt% Al_2O_3, whereas stishovite in the Ono (1998) experiment sh16 at similar *P–T* conditions, contains as little as 0.44 wt% Al_2O_3. Clinopyroxene chemistry in these runs is consistent with each other: $X_{jd} = 0.87$ in run sh16 (Ono, 1998), and $X_{jd} = 0.98$ in our run ma293. However, it was found that garnet in sh16 experiment had a surprisingly low majoritic component (Si = 3.02 cpfu), whereas in our experiment garnet is characterized by Si = 3.14 cpfu, which is consistent with run ma215a (Si = 3.12 cpfu) and ma215b (Si = 3.14 cpfu) performed also at 12 GPa. Other experiments (e.g. sh15 & sh7) conducted by Ono (1998) at 12 GPa produced garnet with Si = 3.09 cpfu, which is much closer to our results than his run sh16. With respect to K-hollandite, our experiments at 9, 10 and 12 GPa, as well as the Ono (1998) experiments at 9 and 12 GPa, are consistent because all of them contain $KAlSi_3O_8$-$NaAlSi_3O_8$ solid solution with a little Fe and/or Ca, whereas at these conditions Irifune *et al*. (1994) produced the pure K-hollandite end member. The first evidence of an $NaAlSi_3O_8$ component in K-hollandite is recorded only at 17.5 GPa and 1500 °C (Irifune *et al*., 1994).

The average volume proportion of garnet in our experiments was 26 vol.% at 9 GPa and 31 vol.% at 12 GPa, while in experiments conducted by others (Ono, 1998) it is ~26 vol.% at 9 GPa and ~28 vol.% at 12 GPa.

DISCUSSION

Our reconnaissance experiments clearly show that the differences in chemical composition and type of starting materials (gel, oxides and mineral mix) cause some discrepancies between the experimental results obtained in different laboratories. However, it has to be stressed that none of the mentioned experiments was reversed, so at this stage they are synthesis results, not an equilibrium. The comparison of our experiments conducted with the starting material corresponding to the real rocks known from UHPM terranes with those performed for the 'average pelite' (Ono, 1998) are partly inconsistent. The extent of such inconsistency cannot be estimated precisely at present because additional experiments are needed. It is assumed however that even small differences in the phase boundaries between hydrous and anhydrous mineral assemblages produced at high pressures and high temperatures may influence the estimate of the depth to which continental metasedimentary rocks may be subducted, the depth at which they still remain buoyant, and the depth at which they exceed the densities of the surrounding mantle. Earlier experiments on the average continental crust and/or sediments have shown that at a depth of about $\geqslant$300 km (pressure $\geqslant$10–11 GPa) the densities of synthetic UHP metamorphic rocks exceed the densities of the surrounding mantle peridotites (Irifune *et al*., 1994). This means that the continental rocks become heavier than mantle rocks and that therefore they will sink down into the mantle transition zone. However, it is not yet clear at what depth this happens or if there is any limit of the depth to which continental rocks may be subducted.

Recent research, involving high-pressure mineral synthesis with *in situ* X-ray diffraction measurements of unit cell parameters, followed by calculations of the densities of synthetic metamorphic rocks through the equation of state, has shown that continental rocks will stop sinking at a depth of ~660 km (Nishiyama *et al*., 2005). These studies have focused on hypothetical continental crust (HCC), the average bulk chemistry of which corresponds to the simplified KMAS system and therefore produces an 'artificial' rock with three minerals – K-hollandite, majoritic garnet and stishovite – in a volume proportion of 1:1:1 (Nishiyama *et al*.,

2005). However, our experiments performed on real UHPM rock compositions show that at 12 GPa the rock already contains ~31 vol.% garnet and still contains ~11 vol.% jadeitic pyroxene; or ~35 vol.% pure jadeite in Na-rich media. Therefore, as pressure increases to the limit where pyroxene is no longer stable, the proportion of garnet is expected to be higher than that proposed for the HCC, because the sodic pyroxene has to be partly dissolved into garnet. The important issue is to understand what phase incorporates Na_2O at very high pressures, the content of which (3.9 wt%) is even greater than K_2O (3.4 wt%) in the average continental crust. It might be expected that Na_2O will be partly dissolved into majoritic garnet (~3 wt% at 21 GPa, see Irifune *et al.*, 1994), and part of the Na will be partitioned into a $KAlSi_3O_8$-$NaAlSi_3O_8$-hollandite solid solution as is observed in our and the Ono (1998) experiments. Although part of the Na may also be incorporated into a partial melt, it is assumed that it will be negligible because the volume of the melt is <1 vol.% at pressures of 16–24 GPa, and such partial melts possess relatively low K/Na ratios and SiO_2 contents (Irifune *et al.*, 1994). Because $KAlSi_3O_8$-$NaAlSi_3O_8$-hollandite solid solutions may be stable at very high pressures as pure end members (e.g. Yagi *et al.*, 1994), their abundance within experimentally synthesized UHP rocks should also be taken into account. Given that the equation of state is sensitive to mineral chemistry, it may be assumed that underestimation of the presence of Na_2O in majoritic garnet and in K-hollandite may partly affect the density calculations and, therefore, the determination of the final 'buoyancy boundary' or 'the point of no return' for deeply subducted metasedimentary rocks.

In addition, it is well known that the continental crust also contains carbonates and metamorphic rocks consisting of a mixture of felsic and carbonate components, pure quartzite or Al-rich quartzites intercalated with felsic gneisses. All of these represent so-called supracrustal lithologies, which are associated with K- and Na-rich granites and diorites, the major constituents of the continental crust. Pure marbles, calc-silicate rocks, felsic gneisses and quartzites containing diamond and coesite are found in UHPM terranes in collisional orogens (e.g. Chopin, 1984; Smith, 1984; Sobolev & Shatsky, 1990; Dobrzhinetskaya *et al.*, 1994, 1995; Ogasawara 2005; Zhang *et al.*, 2002). These types of bulk chemistry also need to be tested by ultra-high pressure experiments, which, we predict, will bring some unexpected results.

Unusual Al-rich quartzites from the Sulu UHPM terrane, China, were recently described by Zhang *et al.* (2002). The quartzite consisted of 70–85 vol.% quartz, 5–20 vol.% kyanite, and 5–15 vol.% topaz-OH, with phengite, rutile and pyrite (all together <3 vol.%). This is the third record of topaz-OH in natural rocks from high-pressure and ultrahigh-pressure metamorphic terranes. Previously, topaz-OH was found in the blueschists of Crete (Theye, 1998) and in quartzite from the UHPM terrane of Dabie and Qinling of China (Kang *et al.*, 1992; Jing *et al.*, 1995). Zhang *et al.* (2002) indicated that topaz-OH from Sulu yields a positive linear correlation between OH content, *a* and *b* unit cell parameters, as well as volume. They used the minimum interval of pressures at which topaz-OH is stable in experiments (Wunder *et al.*, 1993, 1999) and concluded that topaz-OH and its host rocks were metamorphosed in the coesite stability field (650–700 °C, $\geqslant$3 GPa). However, further experimental studies of the topaz-OH stability field has shown that this mineral is stable up to 12 GPa (Schmidt *et al.*, 1998; Sano *et al.*, 2004) within the range of 7–12 GPa and 800–1500 °C. Although the presence of the very-high pressure topaz-OH (8–12 GPa) in metasedimentary rocks incorporated in UHPM continental collision belts is not conclusively documented above the minimum conditions, future studies of such rocks might show that they help to elucidate the 'buoyancy boundary' at which UHP metasedimentary rocks may be exhumed back to the Earth's surface. It will also allow a better understanding of which type of real (not hypothetical) rocks might stagnate at the bottom of the transition zone, which ones might pass through the 660 km discontinuity, and which ones might possibly sink deeper into the lower mantle.

Finally, the densities of hypothetical UHPM rocks calculated by Nishiyama *et al.* (2005), based on the assumption that HCC at the mantle transition zone will consist of an equal amount of majoritic garnet, K-hollandite and stishovite, show that such HCC will be denser than mantle rocks by ~0.2 g cm^{-3} at conditions corresponding to the mantle transition zone. They also showed that at *P–T* conditions below 660 km depth, the HCC rocks will be less dense than surrounding mantle rocks by ~0.15 g cm^{-3}, and therefore they will not sink further into the lower mantle. Nishiyama *et al.* (2005) suggest that the 660 km seismic discontinuity boundary is a place where continental materials are stagnated. These calculations are exciting and impressive, but there is a need for further research in this direction based on reversed experiments and studies of equation of state for each mineral that composes the dominant lithologies of the continental crust. Without looking at a range of natural UHPM rocks and their mineralogical constituents it will not be possible to determine where different lithologies might stop sinking and whether some might penetrate into the lower mantle.

ACKNOWLEDGEMENTS

We thank Y. Wang, J. Zhang and L. Liu for discussions related to ultrahigh-pressure experiments on the felsic starting material and R. Zhang for providing details about natural occurrences of topaz-OH in the Central Chinese Orogenic belt. L.D. especially thanks Prof. Y. Ogasawara for his support and discussions

during her long-term visit to Waseda University. Graduate students from Waseda University, M. Kikuchi and T. Adachi are appreciated for their valuable assistance and help with Raman spectroscopy and EMP analyses. Rigaku Inc. helped to obtain X-ray analyses. We thank F. Forgit for his technical support with the multianvil apparatus. M. Koch-Müller and F. Spear are appreciated for their thoughtful reviews and useful comments. The experimental part of the project was partly supported by NSF grants EAR-0107118 and EAR-02296666. The analytical portion of the run product studies was completed with support to L.D. from the Japanese Society for the Promotion of Science. J. Gilotti is thanked for her editorial comments, and for organizing this special volume.

REFERENCES

Allegre, C. J., Hamelin, B., Provost, A. & Dupre, B., 1987. Topology in isotopic multispace and origin of mantle chemical heterogeneities. *Earth and Planetary Science Letters*, **81,** 319–337.

Armstrong, J. T., 1988. Quantitative analysis of silicate and oxide minerals: comparison of Monte Carlo, ZAF and phi-rho-z procedure. In: *Microbeam Analysis – 1988* (eds Newbury, D.E.), pp. 239–246. San Francisco Press, San Francisco, CA.

Bozhilov, K. N., Xu, Z., Green, H. W. & Dobrzhinetskaya, L. F., 2003b. Exsolution of a phlogopite-10A phases solid solution from diopside in UHPM garnet peridotite from Sulu, China. *GSA, November, 2003, Annual Meeting (Abstract Volume)*, Seattle, Washington. CD-ROM, #219-5 [63946].

Bozhilov, K. N., Green, H. W. & Dobrzhinetskaya, L. F., 1999. Clinoenstatite in the Alpe Arami peridotite: additional evidence of very high pressure. *Science*, **284,** 128–132.

Bozhilov, K. N., Green, H. W. & Dobrzhinetskaya, L. F., 2003a. Quantitative 3D measurement of ilmenite abundance in Alpe Arami olivine: confirmation of high-pressure origin. *American Mineralogist*, **88,** 596–603.

Cesare, B., Marchesi, C. & Connolly, J. A. D., 2002. Growth of myrmekite coronas by contact metamorphism of granitic mylonites in the aureole of Cima di Vila, Eastern Alps, Italy. *Journal of Metamorphic Geology*, **20,** 203–213.

Chopin, C., 1984. Coesite and pure pyrope in high-grade blueschists of the Western Alps: a first record and some consequences. *Contributions to Mineralogy and Petrology*, **86,** 107–118.

Cohen, R. S. & O'Nions, R. K., 1982. Identification of recycled continental material in the mantle from Sr, Nd and Pb isotope investigations. *Earth and Planetary Science Letters*, **61,** 73–84.

Dobrzhinetskaya, L. F., Braun, T., Sheshkel, G. & Podkuiko Yu, A., 1994. Geology and structure of diamond-bearing rocks of the Kokchetav massif (Kazakhstan). *Tectonophysics*, **233,** 293–313.

Dobrzhinetskaya, L. F., Eide, E. A., Larsen, R. B. *et al*. 1995. Microdiamond in high-grade metamorphic rocks of the Western Gneiss Region, Norway. *Geology*, **23,** 597–600.

Dobrzhinetskaya, L. F., Green, H. W. & Wang, S., 1996. Alpe-Arami: a peridotite massif from depth of more than 300 kilometers. *Science*, **271,** 1841–1845.

Dobrzhinetskaya, L. F., Green, H. W., Renfro, A. P., Bozhilov, K. N., Spengler, D. & van Roermund, H. L. M., 2004. Precipitation of pyroxenes and olivine from majoritic garnet: simulation of peridotite exhumation from great depth. *Terra Nova*, **16,** 325–330.

Dobrzhinetskaya, L. F., Green, H. W., Renfro, A. P. & Bozhilov, K. N., 2005. Decompression of majoritic garnet: experimental investigation of the mantle peridotite exhumation. In: *Advances in High-Pressure Technology for Geophysical Applications* (eds Chen, J., Wang, Y., Duffy, T. S., Shen, G. & Dobrzhinetskaya, L. F.), pp. 265–287. Elsevier, Amsterdam.

Dobrzhinetskaya, L. F., Wirth, R. & Green, H. W., 2006. Nanometric inclusions of carbonates in Kokchetav diamonds from Kazakhstan: a new constraint for the depth of their origin. *Earth and Planetary Science Letters*, **243,** 85–93.

Domanik, K. J. & Holloway, J. R., 1996. The stability and composition of phengitic muscovite and associated phases from 5.5 to 11 GPa: implication for deeply subducted sediments. *Geochimica et Cosmochimica Acta*, **21,** 4133–4150.

Domanik, K. J. & Holloway, J. R., 2000. Experimental synthesis and phase relations of phengitic muscovite from 6.5 to 11 GPa in a calcareous metapelite from the Dabie Mountains, China. *Lithos*, **52,** 51–77.

Eggler, D. H. & Baker, D. R., 1982. Reduced volatiles in the system C-O-H: implication to mantle melting, fluid formation, and diamond genesis. In: *High Pressure Research in Geophysics* (eds Akimoto, S. & Manghnami, M. H.), pp. 237–250. Center for Academic Publications, Tokyo.

Green, H. W., Dobrzhinetskaya, L. F., Riggs, E. & Jin, Z-M., 1997. Alpe-Arami: a peridotite massif from the mantle transition zone? *Tectonophysics*, **279,** 1–21.

Harlow, G. E., 2002. Diopside + F-rich phlogopite at high P and T: systematics and the stability of $KMgF_3$, clinochumite and chondrodite. *Geological Materials Research*, **4,** 1–28.

Harlow, G. E. & Davis, R., 2004. Status report on stability K-rich phases at mantle conditions. *Lithos*, **77,** 647–653.

Hart, S. R., Hauri, E. H., Oschman, L. A. & Whitehead, J. A., 1992. Mantle plumes and entrainment: isotopic evidence. *Science*, **256,** 517–520.

van der Hilst, R., Widiayntoro, S. & Engdahl, E. R., 1997. Evidence for deep mantle circulation from global tomography. *Nature*, **386,** 578–584.

Irifune, T., Ringwood, A. E. & Hibberson, W. O., 1994. Subduction of continental crust and terrigenious and pelagic sediments: an experimental study. *Earth and Planetary Science Letters*, **126,** 351–368.

JEOL Ltd, 1993. *Program for ϕ-ρ-Z quantitative analysis*. Instructions XM-87452/Z2328T, 1–7.

Jing, Y. R., Tang, J. F., Gao, T. S. & Hou, M. J., 1995. Study of the ultrahigh-pressure metamorphic minerals, Suson, Anhui. *Geology of Anhui*, **5,** 66–69 (in Chinese).

Kang, W. G., Zhang, S. Y., Liu, X. C. & Qiao, L. Y., 1992. The discovery of kyanite-and-topaz-bearing rocks in high-pressure crustal metamorphic belt of central China and their geological characteristics. *Science in China (Series B)*, **9,** 981–986 [in Chinese].

Luth, R. W., 1997. Experimental study of the system phlogopite-diopside from 3.5 to 17 GPa. *American Mineralogist*, **82,** 1198–1209.

Massonne, H.-J., 1999. A new occurrence of microdiamonds in quartzofeldspathic rocks of the Saxonian Erzgebirge, Germany, and the metamorphic evolution. In: *The P.H. Nixon Volume. Proceedings of 7th International Kimberlitic Conference* (eds Gurney, J. J., Gurney, J. L., Pascoe, M. D. & Richardson, S. H.), pp. 533–539. Red Roof Design CC, Capetown.

Miller, C. F., 1985. Are strongly peraluminous magmas derived from pelitic sedimentary rocks? *Journal of Geology*, **93,** 673–689.

Mposkos, E. D. & Kostopoulos, D. K., 2001. Diamond, former coesite and supersilicic garnet in metasedimentary rocks from the Greek Rhodope: a new ultrahigh-pressure metamorphic province established. *Earth and Planetary Science Letters*, **192,** 497–506.

Nishiyama, N., Rapp, R. P., Irifune, T., Sanehira, T., Yammazaki, D. & Funakoshi, K., 2005. Stability and P-V-T equation of state of $KAlSi_3O_8$-hollandite determined by in situ

X-ray observations and implications for dynamics of subducted continental crust material. *Physics and Chemistry of Minerals*, **32,** 627–637.

O'Neill, H. S. C. & Wood, B. J., 1979. An experimental study of Fe-Mg partitioning between garnet and olivine and its calibration as a geothermometer. *Contribution to Mineralogy and Petrology*, **70,** 59–70.

Ogasawara, Y., 2005. Microdiamonds in ultrahigh-pressure metamorphic rocks. *Elements*, **1,** 91–96.

Ogasawara, Y., Fukasawa, K. & Maruyama, S., 2002. Coesite exsolution from supersilicic titanite in UHP marble from the Kokchetav Massif, northern Kazakhstan. *American Mineralogist*, **87,** 454–461.

Ono, S., 1998. Stability limit of hydrous minerals in sediment and mid-ocean ridge basalt compositions: implications for water transport in subduction zones. *Journal of Geophysical Research*, **103,** 18253–18267.

Ono, S., 1999. High temperature stability of phase Egg $AlSiO_3(OH)$. *Contributions to Mineralogy and Petrology*, **137,** 83–89.

Pawley, A. R., 1994. The pressure and temperature stability limits of lawsonite – implications for H_2O recycling in subduction zones. *Contributions to Mineralogy and Petrology*, **118,** 99–108.

Perraki, M., Proyer, A., Mposkos, E., Kaindl, R. & Hoinkes, G., 2006. Raman micro-spectroscopy on diamond, graphite and other carbon polymorphs from the ultrahigh-pressure metamorphic Kimi Complex of the Rhodope Metamorphic Province, NE Greece. *Earth and Planetary Science Letters*, **241,** 672–685.

Phillips, E. R., 1974. Myrmekite-one hundred years later. *Lithos*, **7,** 181–194.

Plummer, C. C., McGeary, D. & Carlson, D. H., 1999. *Physical Geology*, 8th edn. WCB McGraw-Hill, Boston, MA. 576 pp.

Ringwood, A. E., 1991. Phase transformations and their bearing on the constitution and dynamics of the mantle. *Geochimica et Cosmochimica Acta*, **55,** 2083–2110.

van Roermund, H. L. M. & Drury, M. R., 1998. Ultra-high pressure (P > 6 GPa) garnet peridotites in Western Norway: exhumation of mantle rocks from >185 km depth. *Terra Nova*, **10,** 295–301.

van Roermund, H. L. M., Carswell, D. A., Drury, M. R. & Heijboer, T. C., 2002. Microdiamonds in megacrystic garnet websterite pod from Bardane on the island of Fjortoft, western Norway: evidence for diamond formation in mantle rocks during deep continental subduction. *Geology*, **30,** 959–962.

Sano, A., Ohtani, E., Kubo, T. & Funakoshi, K., 2004. *In situ* X-ray observation of decomposition of hydrous aluminum silicate $AlSiO_3OH$ and aluminum oxide hydroxide d-AlOOH at high pressure and temperature. *Journal of Physics and Chemistry of Solids*, **65,** 1547–1554.

Schmidt, M. W., 1996. Experimental constrains on recycling of potassium from subducted oceanic crust. *Science*, **272,** 1927–1930.

Schmidt, M. W., Finger, L. W., Angel, R. J. & Dinnebier, R. E., 1998. Synthesis, crystal structure, and phase relations of $AlSiO_3OH$, a high pressure hydrous phases. *American Mineralogist*, **83,** 881–888.

Smith, D., 1984. Coesite in clinopyroxene in the Caledonides and its implications for geodynamics. *Nature*, **310,** 641–644.

Sobolev, N. V. & Shatsky, V. S., 1990. Diamond inclusions in garnets from metamorphic rocks: a new environment of diamond formation. *Nature*, **343,** 742–746.

Song, S., Zhang, L., Chen, J., Liou, J. G. & Niu, Y., 2005. Sodic amphibole exsolutions in garnet from garnet-peridotite, North Qaidam UHPM belt, NW China: implications for ultradeep-origin and hydroxyl defects in mantle garnets. *American Mineralogist*, **90,** 814–820.

Spengler, D., van Roermund, H. L. M., Drury, M., Ottolini, L., Maso, P. R. D. & Davies, G., 2006. Deep origin and hot melting of an Archaean orogenic peridotite massif in Norway. *Nature*, **440,** 913–917.

Tarbuck, E. J. & Lutgens, F. K., 2002. *Earth: an Introduction to Physical Geology*, 7th edn. Prentice-Hall, Upper Saddle River, NJ. 670 pp.

Taylor, S. R. & McLennan, S. M., 1985. *The Continental Crust: is Composition and Evolution*. Blackwell, Oxford. 312 pp.

Theye, T., 1998. *Aufsteigende Hochdruckmetamorphose in Sedimemnten der Phyllit-Quarzit-Einbeit Kretas und des Peleponnes*. PhD Dissertation, University of Braunschweig, Braunschweig. 224 pp.

Vernon, R. H., 1978. Pseudomorphous replacement of cordierite by symplectitic intergrowth of andalusite, biotite and quartz. *Lithos*, **11,** 283–289.

van der Voo, R., Spakman, W. & Bijwaard, H., 1999. Mesozoic subducted slabs under Siberia. *Nature*, **397,** 246–249.

Wunder, B., Rubie, D. C., Ross, C. R., Medenbach, O., Seifert, F. & Schreyer, W., 1993. Synthesis, stability and properties of $Al_2SiO_4(OH)_2$: a fully hydrated analogue of topaz. *American Mineralogist*, **78,** 285–297.

Wunder, B., Andrut, M. & Wirth, R., 1999. High-pressure synthesis and properties of OH-topaz. *European Journal of Mineralogy*, **11,** 803–813.

Xu, S. T., Okay, A. I., Ji, S. Y. *et al*. 1992. Diamond from the Dabie-Shan metamorphic rocks and its implication for tectonic setting. *Science*, **256,** 80–82.

Yagi, A., Suzuki, T. & Akaogi, M., 1994. High pressure transitions in the system $KAlSi_3O_8$-$NaAlSi_3O_8$. *Physics and Chemistry of Minerals*, **21,** 12–17.

Yang, J., Xu, Z., Dobrzhinetskaya, L. F. *et al*. 2003. Discovery of metamorphic diamonds in Central China: an indication of a >4000 km-long-zone of deep subduction resulting from multiple continental collisions. *Terra Nova*, **15,** 370–379.

Ye, K., Cong, B. & Ye, D., 2000. The possible subduction of continental material to depth greater than 200 km. *Nature*, **407,** 734–736.

Zhang, J., Li, B., Utsumi, W. & Liebermann, R. C., 1996. In situ X-ray observations of the coesite-stishovite transition: reversed phase boundary and kinetics. *Physics and Chemistry of Minerals*, **23,** 1–10.

Zhang, R. Y., Shu, J. F., Mao, H. K. & Liou, J. G., 1999. Magnetite lamellae in olivine and clinohumite from Dabie UHP ultramafic rocks, central China. *American Mineralogist*, **84,** 564–569.

Zhang, R. Y., Liou, J. G. & Shu, J. F., 2002. Hydroxyl-rich topaz in high-pressure and ultarahigh-pressure kyanite quatzites, with retrograde woodhousite, from the Sulu terrane, eastern China. *American Mineralogist*, **87,** 445–453.

Received 7 May 2006; revision accepted 21 November 2006.